Spring International Engineering Research Journal: ISSN: ISSN-3121-8733, (Volume-13 (Issue): 6, May, Pp 1-21, DOI: 10.4186/ej. Accepted 10th, April, 2026.

Adsorptive and Electrochemical Behaviour *of Abelmoschus esculentus* (Okro) Leaf Extract as a Green Inhibitor for Mild Steel Corrosion in HCl Solutions

[1]Gundat, J. J., [2]Oluwadero, T. A., [3]Ajibade, Z. F., & [4]Okewale, A. O.

[1]Department of Petroleum and Natural Gas Processing, Petreoleum Training Institute, Effurun, Nigeria.
[2]Department of Petroleum Engineering and Geosciences, Petreoleum Training Institute, Effurun, Nigeria.
[3]Department of Petroleum Engineering and Geosciences, Petreoleum Training Institute, Effurun, Nigeria.
[4]Department of Chemical Engineering, Federal University of Petroleum Resources, Effurun, Nigeria

*Corresponding Author: Timothy Ayodeji OLUWADERO, Department of Petroleum Engineering and Geosciences, Petreoleum Training Institute, Effurun, Nigeria.
+2347039409952 e-mail: oluwadero_at@pti.edu.ng

Abstract

The adsorptive and electrochemical behaviour of *Abelmoschus esculentus* (okra) leaf extract as a green corrosion inhibitor for mild steel in hydrochloric acid solutions was investigated. Electrochemical measurements, including open circuit potential, linear polarization resistance, and potentiodynamic polarization, were performed in 1.0, 1.5, 2.0 and 2.5 M HCl within the temperatures of 303, 313, 323 and 333 K. FTIR and GC–MS analyses revealed the presence of tannins, organic acids, and polyphenolic compounds containing hydroxyl, carbonyl, and nitrogen-bearing functional groups responsible for surface adsorption. Inhibition efficiency increased with inhibitor concentration, reaching a maximum of 98.5% at 200 ppm in 1 M HCl, but decreased with increasing temperature, indicating predominantly physical adsorption. Thermodynamic and kinetic analyses yielded activation energy values of 31.06–42.64 kJ·mol^{-1}, with positive enthalpy and negative entropy changes, consistent with endothermic and spontaneous adsorption. Surface morphology and EDX analysis confirmed the electrochemical results. The uninhibited steel showed severe pitting and porous corrosion products, with reduced iron and increased oxygen. In contrast, the inhibited sample exhibited a smoother surface with reduced corrosion damage. EDX detected nitrogen and phosphorus species on the inhibited surface, confirming adsorption of phytochemical constituents and formation of protective organic firm. Adsorption behaviour followed the Langmuir isotherm (R^2 = 0.99), suggesting monolayer coverage on a homogeneous surface. Electrochemical results confirm that *A. esculentus* acts as a mixed-type inhibitor, suppressing both anodic and cathodic reactions through the formation of a protective adsorbed film. The results demonstrate the potential of okra leaf extract as an efficient, environmentally benign inhibitor for mild steel corrosion in acidic media.

Keywords: Corrosion inhibition; *Abelmoschus esculentus*; Mild steel; HCl solution; Adsorption isotherm; Electrochemical behaviour

Accepted: 10/4/2026 Published: 30/5/.2026

1. INTRODUCTION

1.1 Background on Corrosion in Industrial Systems

Corrosion remains a pervasive threat to the integrity, reliability, and safety of oil and gas facilities worldwide [1], [2]. In both upstream and downstream sectors, damage mechanisms arising from corrosive environments can result in equipment failure, production downtime, and significant economic loss[1], [3], [4]. Among the most critical forms of corrosion are acidic and alkaline corrosion, both of which are highlighted in API 571, the

American Petroleum Institute's recommended practice for identifying damage mechanisms in hydrocarbon processing industries.

Despite existing studies on plant-based corrosion inhibitors, there remains limited understanding of the adsorption–structure relationship and thermodynamic behaviour of okra leaf extract under varying acid strengths and temperatures. This study addresses these gaps by integrating electrochemical, thermodynamic, and surface characterisation techniques to provide a comprehensive evaluation of inhibition performance. The novelty of this work lies in the combined application of GC–MS-driven compositional analysis with multi-isotherm modelling and electrochemical validation across industrially relevant acid concentrations.

1.2 Common Corrosive Agents (HCl and NaOH)

Acidic corrosion, typically caused by aggressive species such as hydrochloric acid (HCl), sulfuric acid (H_2SO_4), and organic acids, leads to uniform or localized metal degradation through proton-induced electrochemical attack. In upstream oil and gas production, particularly in onshore, offshore, and deepwater operations, HCl is commonly used in acidizing treatments to enhance reservoir permeability. However, inadequate neutralization and fluid handling can lead to casing and tubing failures due to severe internal corrosion[5]. Similarly, acidic condensates formed in the presence of CO_2 and H_2S in wet gas systems contribute to pipeline degradation and equipment thinning in midstream facilities. In downstream refining operations, acid corrosion is prevalent in crude distillation overheads, catalytic cracking units, and desalter systems where aqueous acidic phases form or accumulate[4], [6]. Understanding the fundamental electrochemical mechanisms governing these acidic corrosion processes is therefore essential for quantifying metal degradation rates and developing effective mitigation strategies.

Corrosion kinetics require at least one anodic and one cathodic half-cell reaction, which proceed independently but occur simultaneously on the metal surface. At the corrosion potential (E_{corr}), the anodic current (I_{anodic}) is equal in magnitude to the cathodic current ($I_{cathodic}$), such that $I_{anodic} = |I_{cathodic}| = I_{corr}$, resulting in a net current of zero. For uniform corrosion, the corrosion current density (i_{corr}) is directly related to the metal loss rate. Polarization resistance (R_p) is defined from the potential–current (E–I) curve as the slope at E_{corr},

$$R_p = \frac{\Delta E}{\Delta I}\Big|_{E=E_{corr}} \quad (1)$$

The theoretical basis for linear polarization resistance (LPR) measurements relies on a Taylor series expansion of the electrode potential–current density relationship [7]. By limiting the degree of polarization, higher-order terms can be neglected;

$$E - E_{corr} \ll \frac{\beta_a}{2.303} \quad (2)$$

$$E - E_{corr} \ll \frac{[\beta_c]}{2.303} \quad (3)$$

Where β_a and β_c are the anodic and the cathodic Tafel slopes for the two half-reactions.

This enabling a linear approximation that leads to the Stern–Geary relationship [8].

$$I_{corr} = \frac{\left(\frac{\beta_a|\beta_c|}{\beta_a+|\beta_c|}\right)}{2.303}\frac{1}{R_p} \quad (4)$$

This relationship provides a direct link between the measured polarization resistance and the corrosion current density, under the condition that the perturbation in potential is sufficiently small to avoid non-linear effects [9], [10]. Therefore, accurate LPR measurements require controlling polarization within a narrow potential range, ensuring that the derived corrosion rates remain valid within the assumptions of the model.

While conventional corrosion inhibitors and materials selection have helped mitigate damage, there is a growing need for environmentally sustainable, cost-effective solutions. In recent years, green corrosion inhibitors derived from plant extracts have gained increasing attention for their biodegradability, availability, and low toxicity. Afia et al. [11] investigated the corrosion inhibition performance of *Allium sativum* (garlic) essential oil on carbon steel in 1 M HCl. Using electrochemical impedance spectroscopy (EIS), Tafel polarization, and weight loss analysis, they demonstrated inhibition efficiency up to 95.8% at room temperature. The inhibition mechanism was attributed to physical adsorption of organosulfur compounds from garlic oil onto the metal surface, following Langmuir adsorption isotherm behaviour.

Similarly, Joycee et al. [12] studied aqueous garlic extract in simulated oil well water (SOWW) environments. With the synergistic addition of Zn^{2+}, an inhibition efficiency of 87% was achieved, and polarization studies indicated the system acted predominantly as a cathodic inhibitor. The study confirmed that *Allium sativum* extract significantly reduced corrosion current density and increased polarization resistance, validating its potential use in multiphase oilfield systems.

Castor plant derivatives have also been extensively examined. Okewale et al. [13] compared the corrosion inhibition effects of ethyl esters of castor seed oil and rubber seed oil in acidic and petroleum-water environments. Their findings indicated that inhibition efficiency decreased with temperature but increased with ester concentration, with rubber seed oil performing slightly better. The adsorption mechanism was physical, and the study applied a factorial design to optimize inhibitor formulation.

Further extending castor's applicability, Santos et al. [14] evaluated the use of castor bark powder (*Ricinus communis*) as an inhibitor for AISI 1020 carbon steel in 0.5 M HCl. Electrochemical analyses, including SVET and

FTIR, indicated that the castor bark offered up to 83% inhibition efficiency, operating as a mixed-type inhibitor through adsorption of oxygen- and nitrogen-containing groups such as ricinoleic acid. This adsorption followed the Langmuir isotherm, consistent with other plant-based inhibitors.

A comprehensive review by Alao et al., [15] synthesized research efforts on the use of green inhibitors in the petrochemical industry. The review highlighted the shift toward plant-based compounds, biopolymers, and even pharmaceutical wastes as sustainable alternatives. Despite encouraging results, with several studies reporting efficiencies above 90%, the review also pointed out unresolved challenges in standardizing inhibitor formulations, understanding adsorption kinetics, and translating laboratory findings into industrial-scale applications.

Within this body of literature, studies on okra leaf extract (*Abelmoschus esculentus*) are relatively recent and fewer in number, though highly promising. Hussein and Khadom [16] reported inhibition efficiencies up to 96% for okra extract in 1 M HCl, confirming that the extract acts as a mixed-type inhibitor. The adsorption followed the Langmuir isotherm, with SEM and FTIR confirming the presence of a protective film.

However, this study builds on this foundation by expanding the scope of investigation in several critical directions. Industrial processes such as acid cleaning, well stimulation, EOR, and CO_2 injection involve varying acid strengths; this study evaluates inhibitor performance across those ranges. Unlike previous work, this study evaluates okra leaf extract in acidic media (HCl) across a broader range of concentrations (1.0–2.5 M) and temperatures (30–60 °C). The study also integrates GC–MS characterization to identify the active chemical constituents and fits the data to multiple adsorption models (Langmuir, Freundlich, Temkin), establishing Langmuir as the most appropriate across all test conditions. Notably, the findings present higher inhibition efficiency in acidic media, with a peak of 98.5% in 1 M HCl.

Other research gaps covered in this recent report include the scarcity of data on thermodynamic parameters; activation energy, enthalpy, and spontaneity of okra-based inhibition, which are evaluated here using Arrhenius and thermodynamic models. Moreover, structure–activity relationships have rarely been investigated through GC–MS; this study applies the technique to identify the functional groups governing inhibition. While previous works relied primarily on FTIR and SEM for surface characterization, this report incorporates quantitative electrochemical metrics, including polarization resistance (*Rp*) and comparative isotherm modeling, to provide a more comprehensive mechanistic understanding.

2. MATERIALS AND METHODS

2.1. Materials

Commercially sourced mild steel coupons measuring 4 cm × 3 cm × 0.14 cm were used as working specimens. Each coupon was initially descaled using a wire brush, smoothed with 120–150 mesh abrasive, and subsequently cleaned with acetone before being air-dried. The elemental composition was identified using X-ray fluorescence (XRF). Prior to experimentation, the surfaces were further polished with progressively finer grades of silicon carbide paper (400–1200 grit), rinsed with distilled water, degreased in ethanol, and stored in a desiccator until use.

Fresh *Abelmoschus esculentus* (okra) leaves were obtained from a local farm in Nigeria. Analytical grade hydrochloric acid (HCl, 37%, Sigma-Aldrich) was employed to prepare the acidic corrosive media, using distilled water.

2.2. Preparation of Inhibitor Extract

The leaves were washed thoroughly with distilled water, air-dried at room temperature for seven days, and milled into fine powder. Soxhlet extraction was performed using Hexane, followed by solvent recovery with a rotary evaporator (ICS, 2008). The resulting concentrate served as stock solution. Working concentrations of 50–200 ppm were prepared by dilution with distilled water immediately before use.

2.3. Preparation of Corrosive Media

Acidic solutions in the range of 1.0–2.5 mol·L^{-1} were prepared from concentrated HCl. All solutions were freshly prepared prior to testing and used under static, aerated conditions.

2.4. Electrochemical Measurements

Electrochemical tests were performed in a conventional three-electrode cell connected to a potentiostat/galvanostat (PGSTAT101, Metrohm Autolab, The Netherlands). The mild steel coupon was used as the working electrode, exposing a surface area of 1.6 cm^2, a graphite rod as the counter electrode, and a silver/silver chloride (Ag/AgCl) as reference. The corrosion behaviour of the mild steel within a temperature range of 30°C to 60°C was assessed in different environments, viz a viz: 1M, 1.5M, 2M and 2.5M of HCl.

Open circuit potential (OCP) was recorded for 30 min before each measurement. Linear polarization resistance (LPR) was obtained by scanning ±10–20 mV about OCP at the potential sweep rate of 1 mV·s^{-1}. Potentiodynamic

polarization curves were measured from –250 to +250 mV vs. OCP at the same scan rate, and corrosion current density (i_{corr}) values were determined from Tafel extrapolation.

All electrochemical measurements were conducted in triplicate to ensure reproducibility, and average values are reported. Standard deviations were calculated and included in graphical representations as error bars.

2.5. Corrosion Rate

The expression for measurement of corrosion rate (CR) in millimetres penetration per year (mm/y) was used to measure corrosion rate (CR) for the specimens, which was expressed in equation 5

$$CR\ (mpy) = \frac{0.13 I_{corr} EW}{d} \quad (5)$$

Where mpy is millimeters per year,
EW is the equivalent weight
d is the density in g/cm^3

2.6. Weight Loss Measurements

Pre-weighed coupons were immersed in 100 mL of test solution at 303–333 K for periods ranging from 24 to 144 h. After exposure, specimens were cleaned, rinsed with distilled water, degreased in ethanol, dried, and reweighed. The corrosion rate (*CR*, mg·cm^{-2}·h^{-1}) was calculated using:

$$CR = \frac{W}{A \times t} \quad (6)$$

where *W* is weight loss (mg), *A* is surface area (cm²), and *t* is immersion time (h).

The inhibition efficiency (*IE*, %) was determined using the linear polarization resistance (LPR), according to:

$$IE, \% = \frac{CR_{blank} - CR_{inh}}{CR_{blank}} \times 100 \quad (7)$$

2.6. Surface Characterization

Surface morphology was examined using scanning electron microscopy (SEM) equipped with energy-dispersive X-ray spectroscopy (EDX). Analyses were performed on selected coupons before and after immersion in corrosive media, both in the absence and presence of the inhibitor.

2.7. Degree of Surface Coverage

The degree of surface coverage (θ) of mild steel by inhibitor molecules was calculated according to [17]:

$$\theta = \frac{I'_{corr} - I_{corr}}{I'_{corr}} \quad (8)$$

where I'_{corr} is the corrosion current density in uninhibited solution, and I_{corr} is the corrosion current density in the presence of inhibitor.

2.8. Film Attractive Power

The film attractive power, expressed as the adsorption equilibrium constant (K_{ads}), was determined from θ values at a given inhibitor concentration and temperature using [18]:

$$K_{ads} \frac{\theta}{C(1-\theta)} \quad (9)$$

2.9. Thermodynamic and Kinetic Models

2.9.1. Activation Energy (E_a)

Activation energy values for mild steel corrosion in the absence and presence of inhibitor were calculated using the Arrhenius equation [19]

$$\ln I_{corr} = -\frac{E_a}{RT} + \ln A \quad (10)$$

where *R* is the universal gas constant (8.314 J·mol^{-1}·K^{-1}), T is absolute temperature (*K*), and *A* is the Arrhenius pre-exponential factor.

2.8.2. Enthalpy and Entropy of Adsorption

The enthalpy (ΔH_{ads}) and the entropy ΔS_{ads} of adsorption were determined from the transition state equation:

$$\log\left(\frac{I_{corr}}{T}\right) = log\left(\frac{R}{Nh}\right) + \frac{\Delta S_{ads}}{2.303\ R} - \frac{\Delta H_{ads}}{2.303\ RT} \quad (11)$$

where *N* is Avogadro's number (6.022 × 10^{23} mol^{-1}) and *h* is Planck's constant (6.626 × 10^{-34} J·s).
The Gibbs free energy of adsorption (ΔG_{ads}) was related to K_{ads} [20]:

$$\Delta G_{ads} = -RTln\ (55.5 K_{ads}) \quad (12)$$

where 55.5 represents the molar concentration of water in the solution.

3.0 RESULTS AND DISCUSSION

3.1 Characterization of Okro Leaf (*Alelmoschus esculentus*) Extract

3.1.1 Fourier Transform Infrared Spectroscopy (FTIR)

The Fourier Transform Infra-Red (FT–IR) spectrum of *Abelmoschus esculentus* leaf extract (Figure 1) revealed characteristic absorption bands corresponding to hydroxyl (–OH), carbonyl (C=O), amine (N–H), nitrile (C≡N), alkyne (C≡C), aromatic C=C, and C–O groups, confirming the presence of polyphenolic, nitrogenous, and sulfur-containing phytochemicals. These functional groups, particularly those containing oxygen, nitrogen, and sulfur, act as active adsorption centers on steel surfaces due to their electron-donating capabilities from lone pairs and π-electrons. Such interactions facilitate the

formation of protective organo-metallic complexes and adsorbed films that suppress both anodic and cathodic corrosion reactions. The observed spectrum, therefore, supports the role of okra leaf extract as a corrosion inhibitor, in agreement with previous studies attributing inhibitive properties of plant-derived extracts to the combined action of hydroxyl, carbonyl, and heteroatom-containing groups [3], [21], [22], [23]

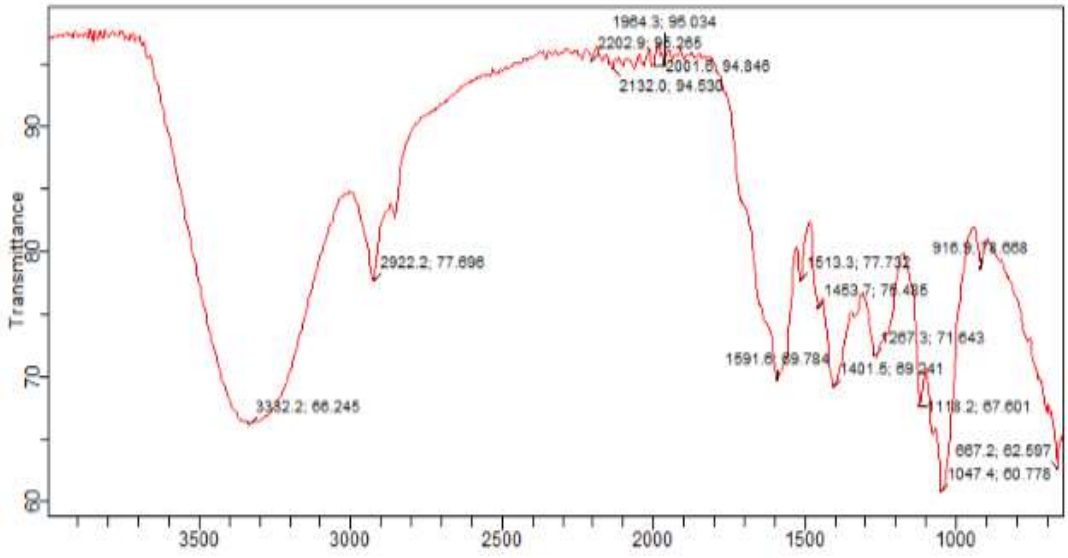

Figure 1: *FTIR Analysis Result of Okro leaf extract*

3.1.2 Chemical Constituents of *Alelmoschus esculentus*

Gas Chromatography–Mass Spectrometry (GC–MS) analysis of *Abelmoschus esculentus* leaf extract revealed a complex chemical profile dominated by tannins and organic acids (Figure 2 and 3). The chromatograms exhibited multiple well-resolved peaks across the retention time range, particularly in the mid- to late-elution window, which is consistent with the presence of polyphenolic compounds such as tannins. Mass spectral deconvolution confirmed the abundance of tannin molecules characterized by multiple hydroxyl and carboxyl groups, along with low-molecular-weight organic acids showing distinctive carboxylate fragments. A blank run confirmed the absence of extraneous signals, verifying that the identified peaks are intrinsic to the extract. These findings demonstrate that the extract contains chemically active phytochemicals capable of surface interaction and corrosion mitigation.

The predominance of tannins is particularly significant for corrosion inhibition. Due to their polar hydroxyl and carboxyl functionalities, tannins adsorb strongly onto metallic surfaces, where they form a protective film that limits contact between the steel substrate and aggressive species in the electrolyte. This adsorption process reduces the anodic dissolution of iron and retards access of protons and chloride ions to the surface, thereby suppressing corrosion. In addition, the organic acids detected in the extract play a complementary role. By coordinating with iron centers on the steel surface and scavenging reactive hydroxyl radicals in the corrosive medium, these acids reduce the reactivity of the electrolyte and stabilize the protective film formed by tannins. Together, these compounds produce a mixed-mode inhibition mechanism, with tannins providing the bulk of the barrier effect and organic acids enhancing stability and chemical resistance.

The combined action of tannins and organic acids explains the reduced corrosion rate observed in inhibited systems compared with the blank. These results align with previous reports on plant-derived inhibitors [21], [24], which emphasize the central role of polyphenols and organic acids in adsorption-driven protection. The synergistic effects of these phytochemicals highlight the potential of *A. esculentus* extract as an environmentally friendly corrosion inhibitor. While GC–MS has provided valuable insight into the identity of the active components, further electrochemical and surface studies are recommended to quantify adsorption efficiency, characterize the protective layer, and establish a direct correlation between inhibitor concentration and corrosion performance.

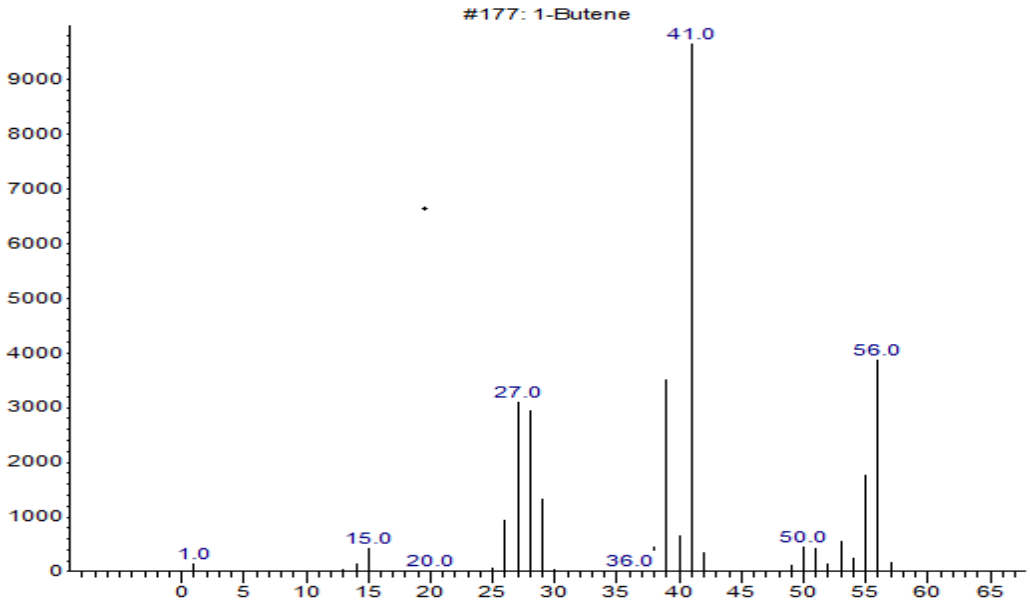

Figure 2: *GC-MS result analysis for Okro leaf extract*

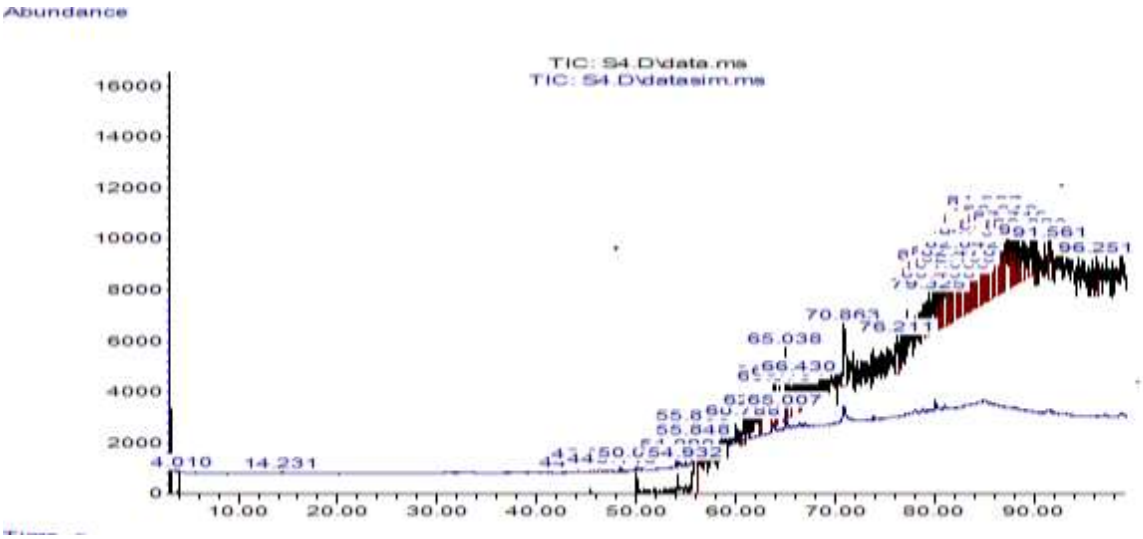

Figure 3: *Total Ion Chromatogram (TIC) of Abelmoschus esculentus leaf extract obtained by GC–MS. The profile shows multiple well-resolved peaks across the retention time range (40–100 min), corresponding predominantly to tannins and organic acids. The abundance and distribution of peaks reflect the complex phytochemical composition of the extract*

3.2 Corrosion Studies Using Electrochemical Method in Acidic Medium

3.2.1 Corrosion Studies Using Electrochemical Method in Acidic Medium

Figures 4(a)–4(d) present the variation of inhibition efficiency with inhibitor concentration for mild steel corrosion in acidic media at temperatures between 303 and 333 K. The results show that increasing the concentration of *A. esculentus* extract enhances adsorption of active molecules onto the steel surface, thereby reducing the effective contact between the metal and the corrosive environment. This leads to higher inhibition efficiencies and lower weight loss, consistent with earlier findings by Yawas [23] and Nwabanne and

Okafor (2011). The improvement in performance with concentration is attributed to accelerated adsorption kinetics and rapid formation of a protective film on the metal surface [25]. However, the efficiency increase is most pronounced between 50 and 150 ppm, beyond which further addition of extract produces only marginal improvement. At concentrations above 200 ppm, the inhibition efficiency approaches a plateau, reflecting a saturation effect where the metal surface becomes largely covered and additional molecules contribute little to further protection.

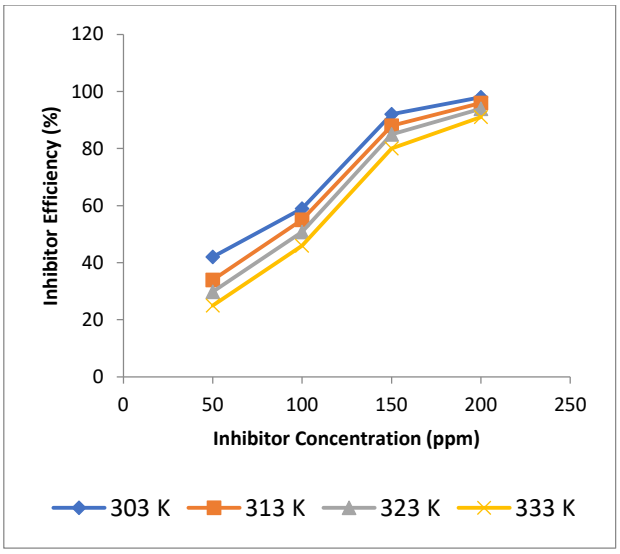

Figure 4 (a): *Plot of inhibitor efficiency against inhibitor concentration at various temperatures in 1 M HCl*

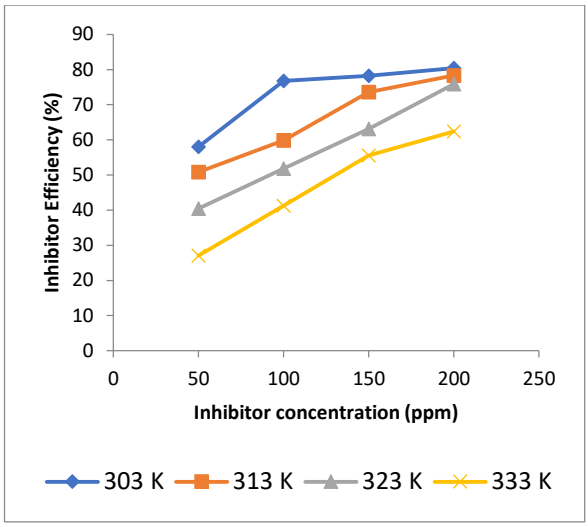

Figure 4 (b): *Plot of inhibitor efficiency against inhibitor concentration at various temperatures in 1.5 M HCl*

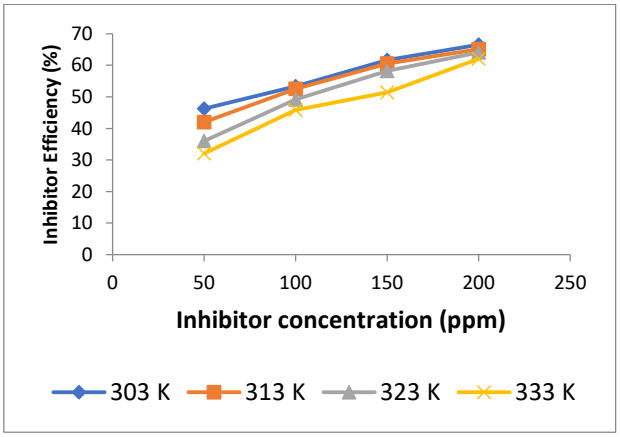

Figure 4 (c): *Plot of inhibitor efficiency against inhibitor concentration at various temperatures in 2 M HCl*

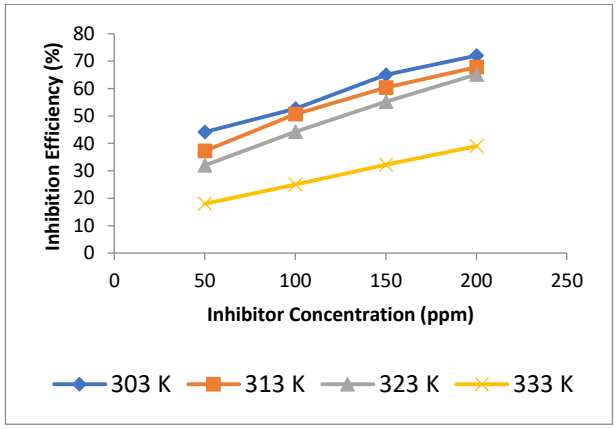

Figure 4 (d): *Plot of inhibitor efficiency against inhibitor concentration at various temperatures in 2.5 M HCl*

Figures 5 (a) – 5 (c) present the variation of corrosion rate with inhibitor concentration for mild steel in acidic media at temperatures ranging from 303 to 333 K. The results indicate a progressive decline in corrosion rate as the concentration of okro extract increased from 50 to 200 ppm. This trend is ascribed to enhanced adsorption of active phytochemical constituents onto the steel surface, leading to the formation of a protective thin film that mitigates direct interaction with the corrosive environment. Such behavior corroborates earlier observations reported by Yawas [23], Nwabanne and Okafor [26], and Kairi and Kassim [19].

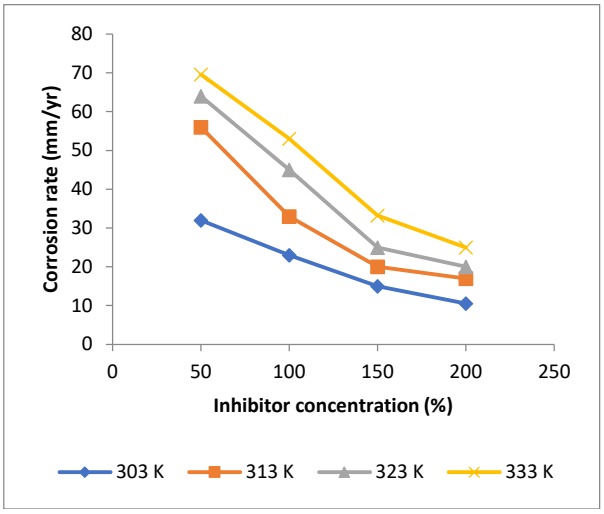

Figure 5 (a): *Plot of corrosion rate against inhibitor concentration at various temperatures in 1 M HCl*

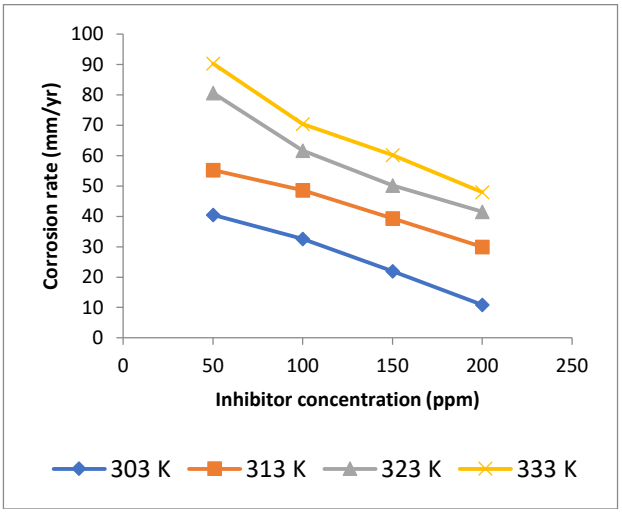

Figure 5 (b): *Plot of corrosion rate against inhibitor concentration at various temperatures in 1.5 M HCl*

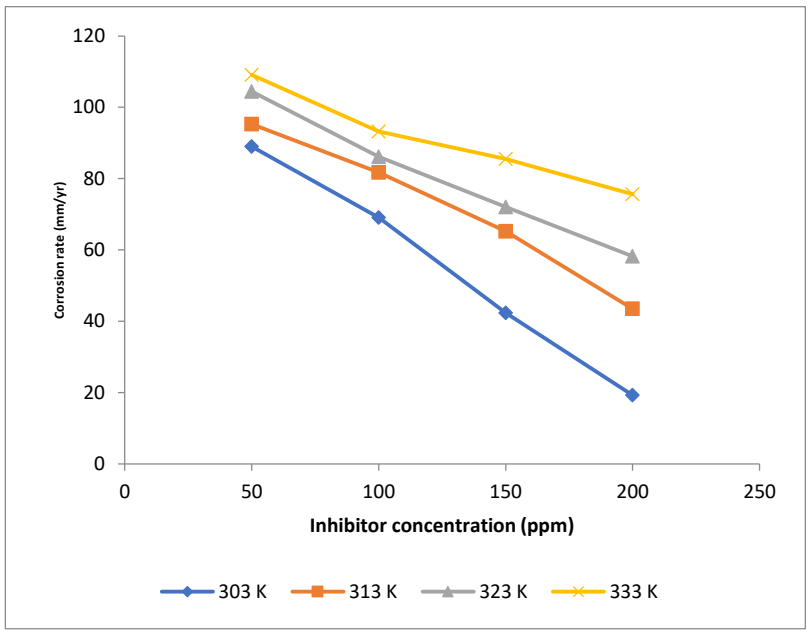

Figure 5 (c): *Plot of corrosion rate against inhibitor concentration at various temperatures in 2.5 M HCl*

3.2.2 Effect of Temperature in Acidic Medium

Figures 5 (a)–5 (d) show that the inhibition efficiency of okro leaf extract decreases with increasing temperature in acidic media at fixed concentrations. For instance, in 1 M HCl, efficiency at 50 ppm dropped from ~44% at 303 K to ~9% at 333 K, while at 100 ppm it declined from ~52% to ~18%. Similar behavior was observed at higher dosages (150–200 ppm) and in more concentrated acids (1.5–2.5 M HCl). This trend indicates reduced stability of adsorbed inhibitor molecules at elevated temperatures, with desorption becoming dominant above 333 K. These observations, consistent with Miralrio and Vázquez [27] and Okewale and Adebayo (2020), suggest the extract is most effective below 333 K.

Figures 5 (a)–5 (c) highlight the effect of temperature on corrosion rate. In 1 M HCl with 50 ppm inhibitor, corrosion rate rose from 32 mm/yr at 303 K to 53 mm/yr at 333 K, compared with a sharp increase from 55 mm/yr to 151 mm/yr for the blank. Similar patterns were observed at

other concentrations and acid strengths. A slight decline in the blank after 323 K likely resulted from corrosion product buildup, partly shielding the surface [28].

Collectively, these results confirm that corrosion rate increases with temperature, while inhibitor efficiency decreases, consistent with a physical adsorption mechanism. Desorption of inhibitor molecules at elevated temperatures exposes more steel surface to attack, as similarly reported by Abd El-Hameed [29].

3.2.3 The Kinetic Parameter of Activation in Acidic Medium

Figures 6–7 present the plots of log corrosion current density (i_{corr}) versus the inverse of absolute temperature, yielding linear relationships as described by equation 10**.** From the slopes ($-E_a$/2.303R), activation energies were determined for each inhibitor concentration, with the results summarized in Table 1.

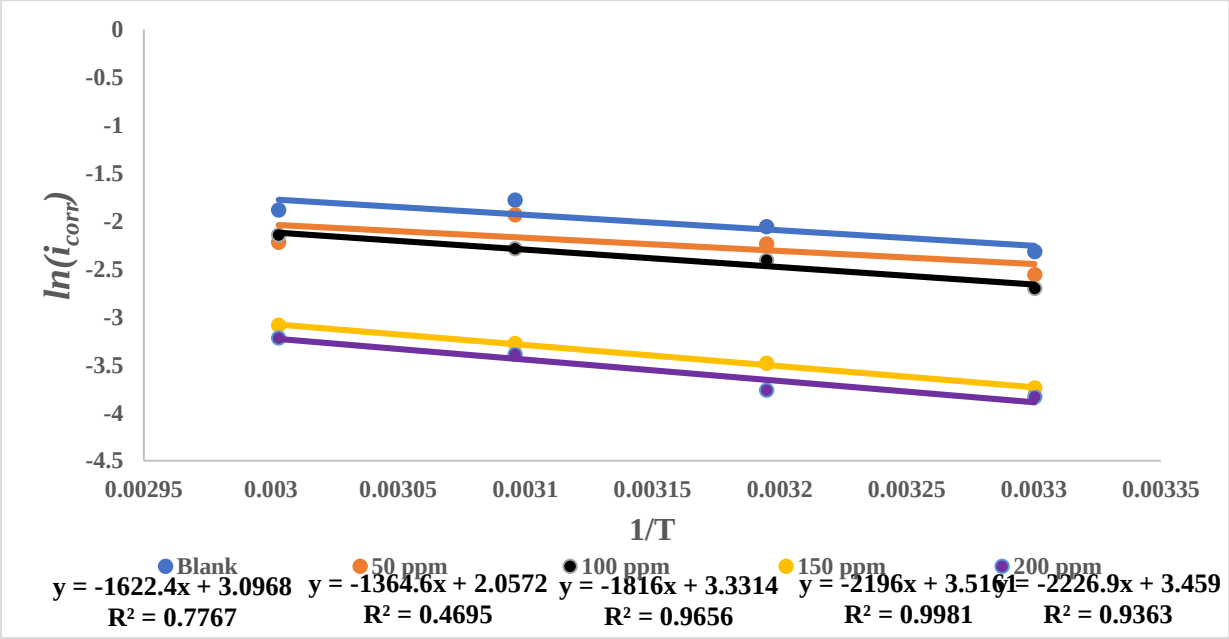

Figure 6: *Plot of Log (i_{corr}) against 1/T in Acidic medium*

Table 1: Showing the activation energy at different inhibitor concentration in acidic medium

Inhibitor Concentration	Activation Energy,E_a(KJ/mol)
50 ppm	32.12
100ppm	34.77
150ppm	42.05
200ppm	42.64
Blank	31.06

The activation energy values ranged from 31.06 kJ/mol in the absence of inhibitor to 42.63 kJ/mol at 200 ppm inhibitor concentration. The higher activation energy observed for the protected metal compared to the blank indicates retardation of mild steel corrosion in the presence of the extract. This increase in activation energy suggests that the energy barrier to corrosion rises with inhibitor concentration, consistent with the findings of Eddy et al., [30].

Furthermore, the activation energies obtained are below the 80 kJ/mol threshold generally associated with chemisorption [30]. Since chemisorption typically involves higher activation energy than physisorption [27], [31], the relatively low values observed confirm that the adsorption of okro extract molecules on the mild steel surface proceeds predominantly through physical adsorption.

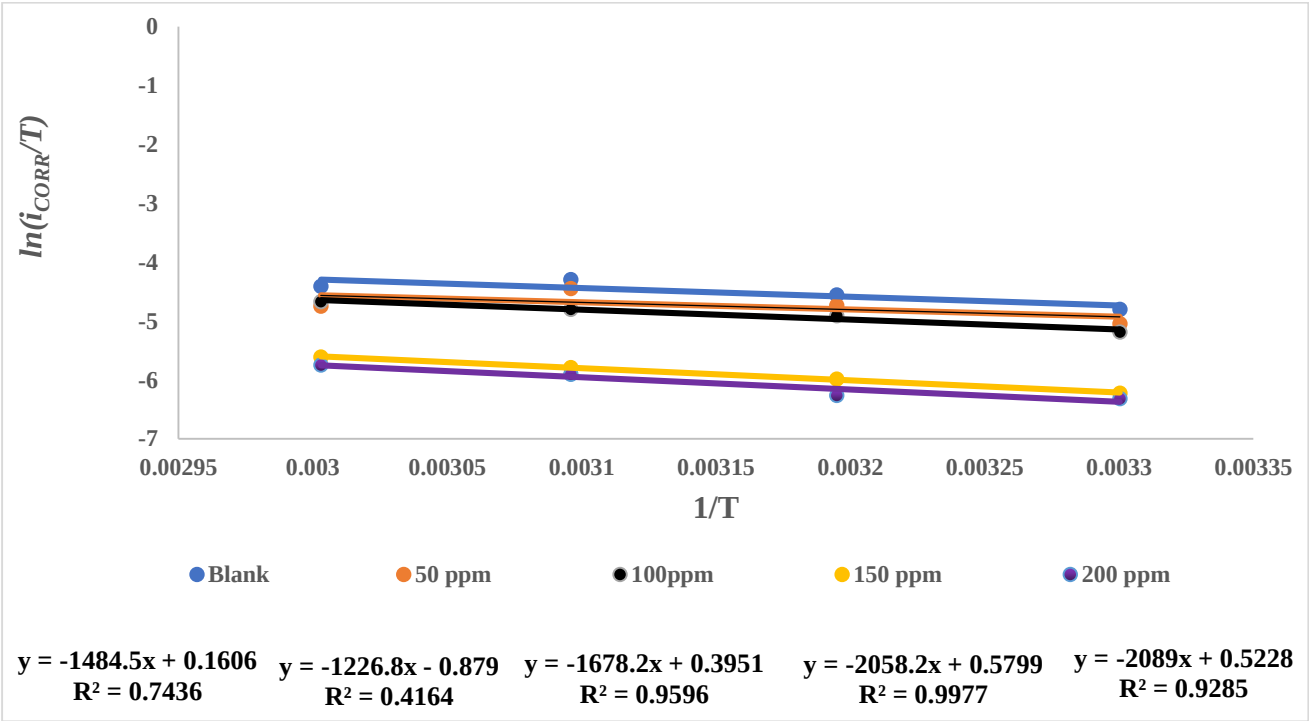

Figure 7: A plot of ln(icorr/T) against 1/T in acidic medium

Furthermore, as expressed by equation 11, the relationship between ln (i_{corr}/T) and *1/T* is depicted by Figure 7

To evaluate the enthalpy (*ΔH*) and entropy (*ΔS*) of inhibitor adsorption on mild steel in acidic medium, the slope and intercept of equation 11 were derived from the plot shown in Figure 7. The calculated thermodynamic parameters are presented in Table 2. The positive *ΔH* value indicates an endothermic adsorption process, while the negative *ΔS* value reflects a decrease in system randomness, suggesting that the adsorbed species are more ordered than the free molecules in solution. In cases of chemisorption, a negative *ΔS* ($\Delta S < 0$) implies that the products formed possess lower entropy compared to the initial reactants.

The calculated values of ($E_a - \Delta H_a$) in Table 4.3 are close to *RT* (2.67 kJ/mol), indicating that the inhibitor exerted a comparable effect on both E_a and ΔH_a, consistent with the findings of Zarrouk et al. [32]. The observed increase in E_a in the presence of inhibitor suggests a mechanism dominated by physical adsorption, as a higher energy barrier in inhibited systems typically reflects weak chemical interactions or physisorption between the inhibitor molecules and the steel surface. According to Szauer and Brand, this rise in activation energy can be attributed to reduced adsorption of inhibitor species at elevated temperatures, which consequently exposes more metal surface to the corrosive medium and accelerates corrosion.

The enthalpy of activation (ΔH_a) values were positive both in the absence and presence of inhibitor, confirming that the dissolution of mild steel is an endothermic process. Moreover, the higher ΔH_a values obtained in inhibited solutions compared to the blank reflect the protective action of the extract, corresponding to a slower dissolution rate and reduced corrosion of mild steel. These findings are consistent with the thermodynamic relationship linking ΔG_a, E_a, and ΔH_a.

Table 2: Thermodynamic parameter of adsorption for acidic medium

E_a (KJ/mol)	ΔH (KJ/mol)	ΔS (KJ/molK)	$E_a - \Delta H$
32.12	28.48	-0.1570	3.64
34.77	32.13	-0.1326	2.64
42.05	39.40	-0.1290	2.67
42.64	39.99	-0.1301	2.64
31.06	23.42	-0.1371	7.64

However, it is important to note that activation energy alone is not sufficient to definitively distinguish between

physisorption and chemisorption. Therefore, it must be interpreted alongside adsorption and thermodynamic data.

3.3 Adsorption Isotherm Analysis

The adsorption behaviour of the inhibitor on the metal surface in 2.5 M HCl was analysed using Langmuir, Freundlich, and Temkin isotherm models.

Langmuir adsorption isotherm

The Langmuir model assumes monolayer adsorption onto a homogeneous surface and is expressed as:

$$\frac{C}{\theta} = \frac{1}{K_{ads} q_m} + \frac{C}{q_m} \quad (13)$$

where C is the inhibitor concentration, θ is the surface coverage, q_m is the monolayer adsorption capacity, and K_{ads} is the equilibrium constant.

Plots of C/θ versus C (Fig. 8) gave linear relationships with high regression coefficients (R^2 = 0.91–0.99, Table 4.5). The calculated K_{ads} values decreased with temperature (0.0118 mol^{-1} at 303 K to 0.0089 mol^{-1} at 333 K), indicating stronger adsorption at lower temperatures. Slopes less than unity suggest attractive interactions between adsorbed molecules, confirming good adherence to the Langmuir model.

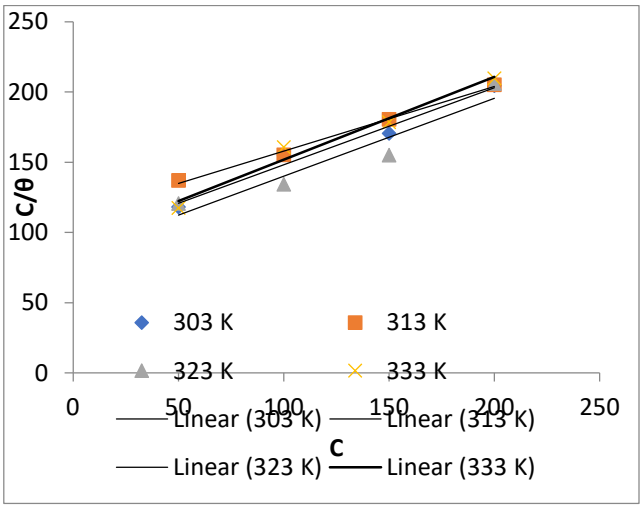

Figure 8*: Langmuir Adsorption Isotherm*

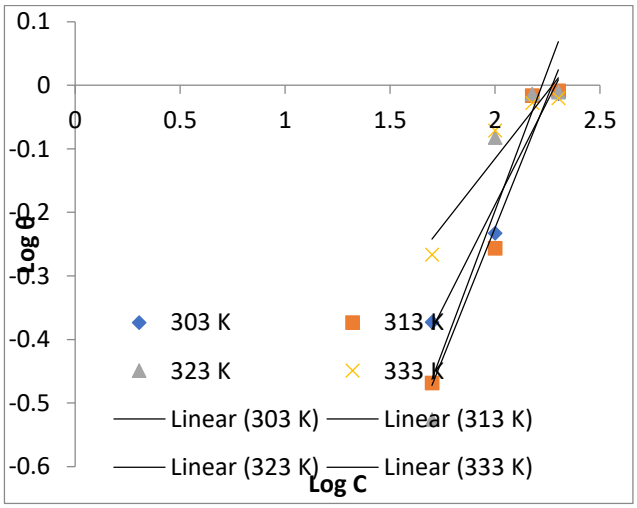

Figure 9: *Freundlich Adsorption Isotherm*

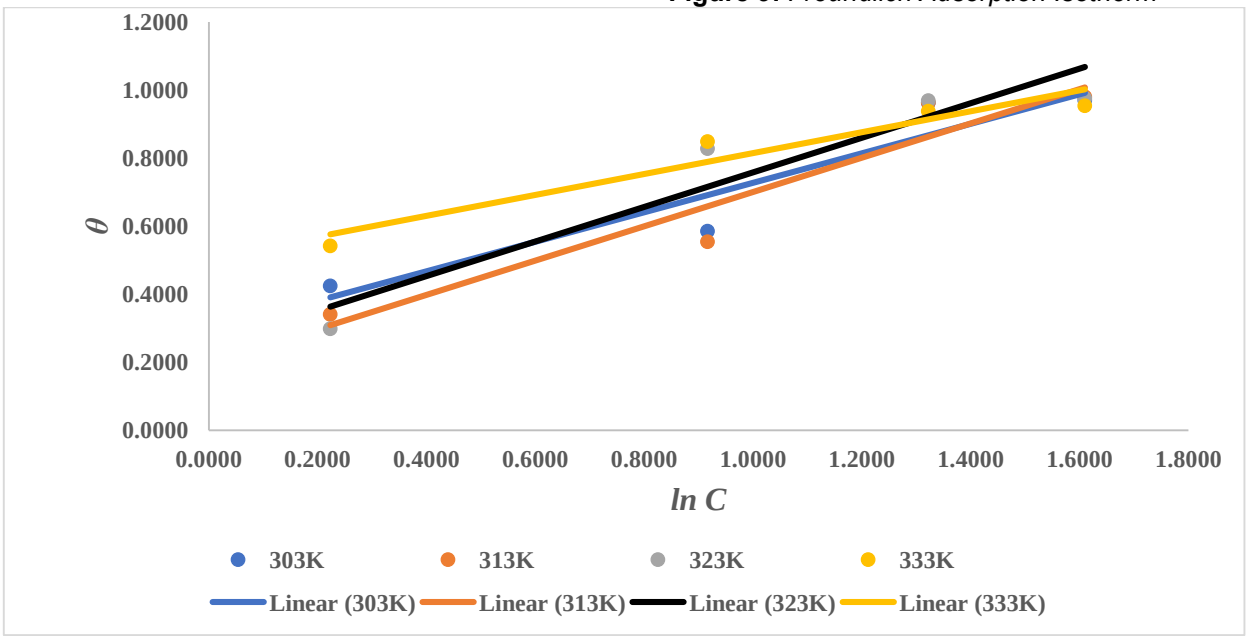

Figure 10 *Temkin Adsorption Isotherm*

Freundlich adsorption isotherm

The Freundlich model accounts for adsorption on a heterogeneous surface with non-uniform energy distribution and is given by:

$$ln\theta = lnK_F + \frac{1}{n} lnC \quad (14)$$

where K_F is the Freundlich constant and *n* the adsorption intensity.

Linear plots of $ln\theta$ versus *ln* C (Fig. 9) showed correlation coefficients between 0.87 and 0.96, confirming a good fit. Since $n \neq 1$, adsorption was non-ideal, suggesting multilayer adsorption and surface heterogeneity [33], [34].

Temkin adsorption isotherm

The Temkin model considers adsorbate–adsorbent interactions and assumes that the adsorption heat decreases linearly with surface coverage. It is represented as:

$$\theta = \frac{RT}{b} lnK_T + \frac{RT}{b} lnC \quad (15)$$

where K_T is the equilibrium binding constant, *b* is related to the adsorption heat, *R* is the universal gas constant, and *T* is absolute temperature.

Plots of θ versus *ln* C (Figure 10) gave regression coefficients above 0.90. The equilibrium constants increased with temperature, reaching 5.20 mol^{-1} at 333 K, consistent with the Temkin assumption of decreasing adsorption heat with increasing surface coverage.

Adsorption isotherm analysis was performed using Langmuir, Freundlich, and Temkin models to describe the interaction between inhibitor molecules and the metal surface. The Langmuir adsorption isotherm suggested monolayer adsorption with reasonable linearity, indicating that inhibitor molecules occupy active sites on the steel surface. However, the use of concentration in ppm introduces limitations, and the resulting adsorption constant should be regarded as an apparent parameter rather than a strict thermodynamic equilibrium constant due to the multi-component nature of plant extracts. The Temkin adsorption isotherm provided a better representation of the system, indicating that interactions between adsorbed species are significant and that adsorption energy decreases with increasing surface coverage. Similarly, the Freundlich model confirmed surface heterogeneity and the possibility of multilayer adsorption.

Collectively, these results indicate that adsorption occurs on a heterogeneous mild steel surface and is not strictly ideal, with Temkin and Freundlich models providing a more realistic description than Langmuir alone.

3.4 Electrochemical Investigations

3.4.1 Potentiodynamic Polarisation Behaviour

The polarisation behaviour of mild steel in 2.5 M HCl, both in the absence and presence of varying concentrations (50–200 ppm) of *Abelmoschus esculentus* (okra) leaf extract, is presented in Figures 11–14, while Table 3 summarised the result for Polarization resistance (*Rp*) values, calculated using the Stern–Geary equation based on the estimated anodic and cathodic Tafel slopes. The linear sweep voltammetry (LSV) curves show a consistent decrease in both anodic and cathodic current densities upon the addition of the inhibitor, indicating that the extract effectively suppresses anodic metal dissolution and retards the cathodic hydrogen evolution reaction. In the anodic region, a linear segment of the curve was observed for all inhibitor concentrations, corresponding to controlled dissolution at low overpotentials. Beyond a critical potential, the anodic current rose sharply, attributed to the desorption of adsorbed inhibitor molecules from the steel surface, a behaviour consistent with earlier reports on iron in acidic media [35].

Quantitative polarisation parameters further support this inhibition mechanism. The corrosion current density (i_{corr}) and corrosion rate (CR) decreased markedly with increasing inhibitor concentration, accompanied by an increase in polarisation resistance (*Rp*). At 303 K, the corrosion rate declined from 114.43 mm yr^{-1} for the blank to 19.35 mm yr^{-1} at 200 ppm, signifying strong surface protection. The corrosion potential (E_{corr}) shifted slightly towards more noble values, confirming mixed-type inhibition with a predominant influence on the anodic process.

Temperature variation between 303 and 333 K revealed an increase in both anodic and cathodic current densities with rising temperature in inhibited and uninhibited systems alike, resulting in higher corrosion rates and reduced inhibition efficiency. This temperature dependence suggests that adsorption of the okra extract constituents occurs mainly through physical adsorption, which weakens at elevated temperatures due to desorption of adsorbed species.

Overall, the okra leaf extract exhibited significant corrosion inhibition efficiency in acidic medium by forming an adsorbed protective film on the steel surface, reducing charge transfer at the metal–solution interface. The observed decline in inhibition efficiency with temperature reinforces the predominance of a physisorption-controlled mechanism.

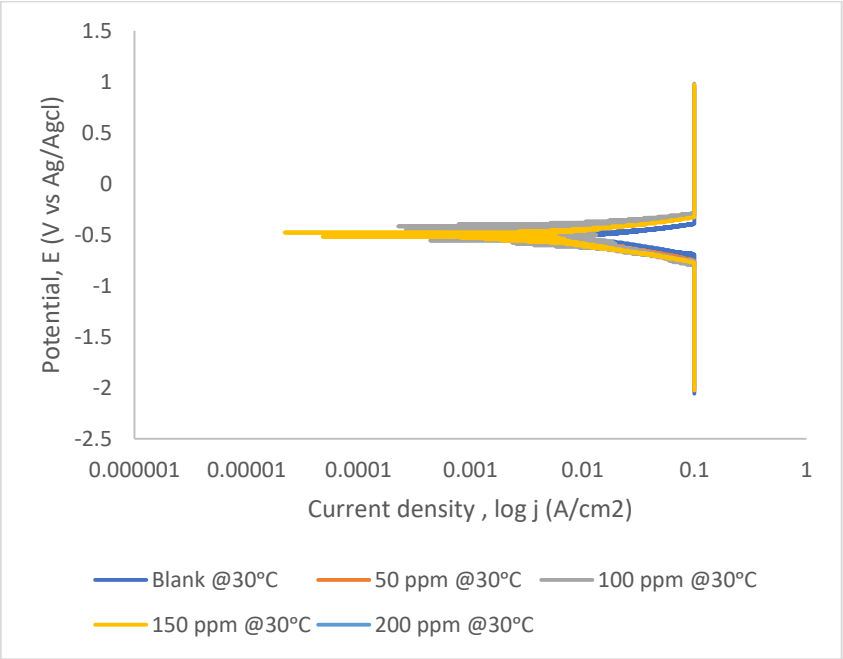

Figure 11: *Tafel plot of Polarization curves of mild steel in 2.5M HCl in the presence of different concentrations of inhibitor at 30 °C using LSV*

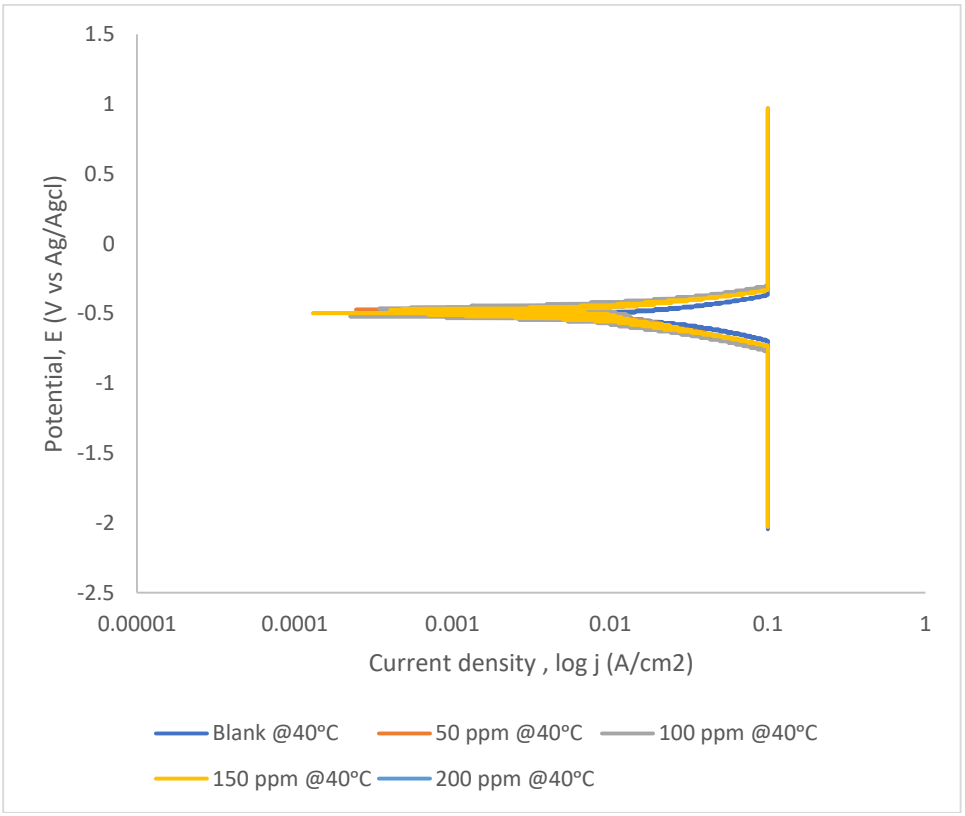

Figure 12: *Tafel plot of Polarization curves of mild steel in 2.5M HCl in the presence of different concentrations of inhibitor at 40 °C using LSV*

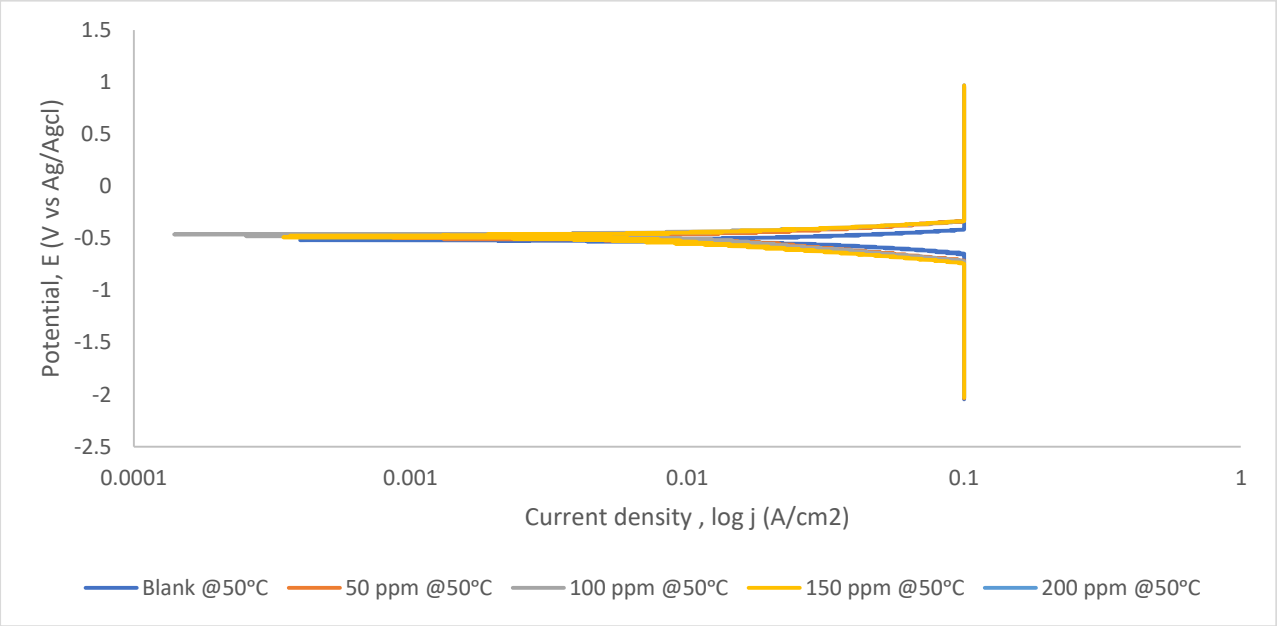

Figure 13: *Tafel plot of Polarization curves of mild steel in 2.5M HCl in the presence of different concentrations of inhibitor at 50 °C using LSV*

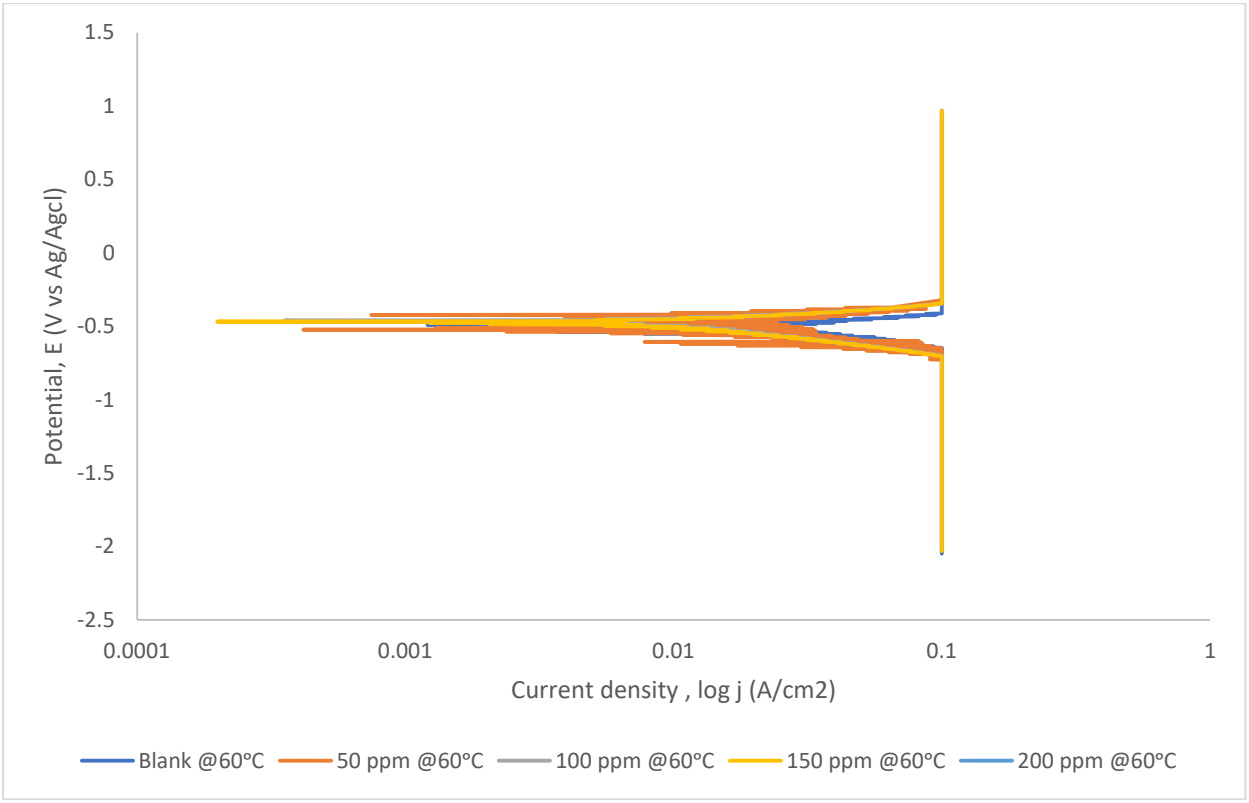

Figure *14:* *Tafel plot of Polarization curves of mild steel in 2.5M HCl in the presence of different concentrations of inhibitor at 60 °C using LSV*

Table 3: *Potentiodynamic polarization parameters for corrosion of mild steel in 2.5 M HCl with various concentrations of okro leave extract and temperatures.*

303K					
Inhibitor concentration(ppm)	E_{corr} **(V)**	$j_{corr} = \lvert j_{meausured} \rvert$ **(A/cm²)**	I_{corr} **(A)**	**CR (mm/yr)**	R_P **(Ω.cm²)**
Blank	-0.53489	0.00631902	0.006319	114.4267	4.12369
50	-0.52414	0.000782816	0.00078	89.0281	33.2871
100	-0.54431	0.00645152	0.00645	64.1881	4.039
150	-0.51992	0.00707302	0.007073	52.9663	3.68409
200	-0.48865	0.00166527	0.001665	19.3503	15.6477
313K					
Inhibitor concentration(ppm)	E_{corr} **(V)**	$j_{corr} = \lvert j_{meausured} \rvert$ **(A/cm²)**	I_{corr} **(A)**	**cr (mm/yr)**	R_P **(Ω.cm²)**
Blank	-0.52108	0.0147488	0.014749	131.38	1.76677
50	-0.48722	0.00820933	0.008209	95.3919	3.17415
100	-0.51983	0.0199421	0.019942	81.726	1.30666
150	-0.49834	0.00167571	0.001676	69.4717	15.5502
200	-0.52122	0.00504164	0.005042	43.5836	5.16849
323K					
Inhibitor concentration(ppm)	E_{corr} **(V)**	$j_{corr} = \lvert j_{meausured} \rvert$ **(A/cm²)**	I_{corr} **(A)**	**CR (mm/yr)**	R_P **(Ω.cm²)**
Blank	-0.51983	0.0199421	0.019942	171.726	1.30666
50	-0.49372	0.00511892	0.005119	104.4815	5.09047
100	-0.46831	0.00386524	0.003865	82.9138	6.74155
150	-0.47891	0.00361814	0.003618	72.0425	7.20196
200	-0.48689	0.00975	0.00975	58.294	2.67258
333K					
Inhibitor concentration(ppm)	E_{corr} **(V)**	$j_{corr} = \lvert j_{meausured} \rvert$ **(A/cm²)**	I_{corr} **(A)**	**CR (mm/yr)**	R_P **(Ω.cm²)**
Blank	-0.52888	0.378211	0.37821	173.79	0.0689
50	-0.51109	0.0287541	0.028754	109.121	0.906226
100	-0.46988	0.00716479	0.007165	93.2545	3.6369
150	-0.47681	0.00736541	0.007365	85.5856	3.53784
200	-0.46802	0.0082317	0.008232	75.6519	3.16553

3.5 Surface Morphology Analysis

3.5.1 SEM-EDX Analysis

The differences in surface morphology and elemental composition of mild steel exposed to 2.5 M HCl in the absence and presence of *Abelmoschus esculentus* leaf extract reflect the key interfacial processes governing corrosion and inhibition under acidic conditions.

The polished, unexposed steel surface (Figure 15) exhibits a smooth, uniform morphology with no pits or

corrosion features. The corresponding EDX spectrum shows a dominant iron content of 72.55 wt%, with negligible oxygen, confirming the absence of surface oxidation and providing a baseline for assessing corrosion-induced changes.

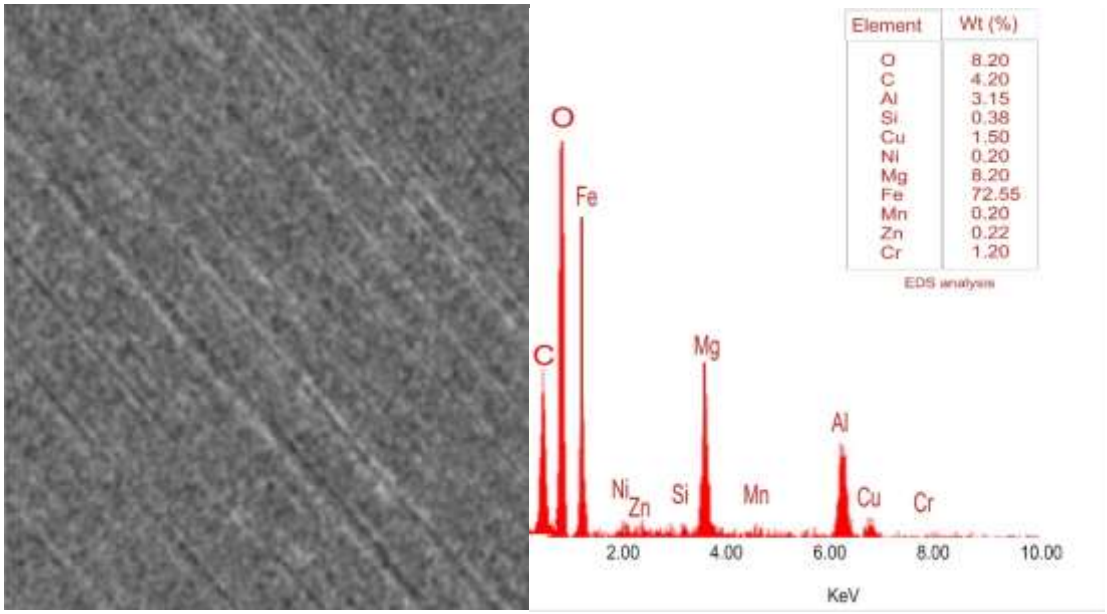

Figure 15: *SEM and EDX data of mild steel that is not dip in acidic medium.*

Upon immersion in uninhibited 2.5 M HCl, the steel surface (Figure 16) suffers severe degradation, characterised by extensive roughening, deep pits, and porous corrosion products extending along grain boundaries. These features indicate aggressive chloride-induced corrosion, where chloride ions adsorb on the steel surface, destabilise transient oxides, and promote localized anodic dissolution. Grain boundaries, being electrochemically active, serve as preferential anodic sites, facilitating pit growth and intergranular attack. EDX analysis of this uninhibited sample surface (Figure 17) reveals reduced iron and elevated oxygen content, consistent with the formation of iron oxides and hydroxides. The porous and non-adherent nature of these products allows continuous electrolyte access, sustaining active corrosion. These morphological features are consistent with the observations of Abdallah et al. [36], Makhtar et al. [37], and Alao et al. [15], who similarly reported severe surface damage in uninhibited acidic environments

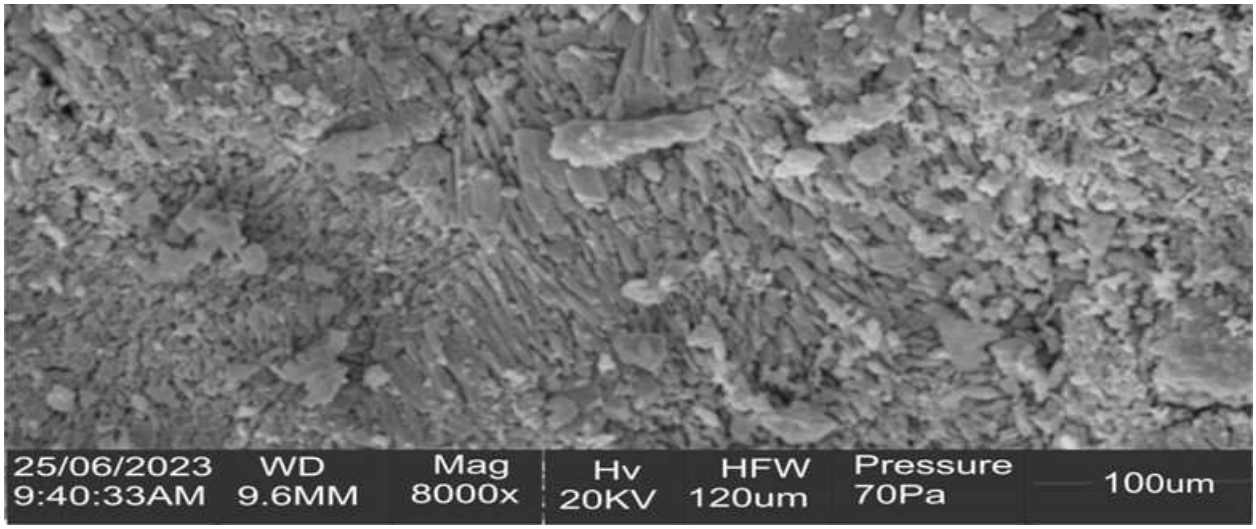

Figure 16: *(Plate XIII) Micrograph of mild steel that is dip in 2.5M HCL medium without inhibitor*

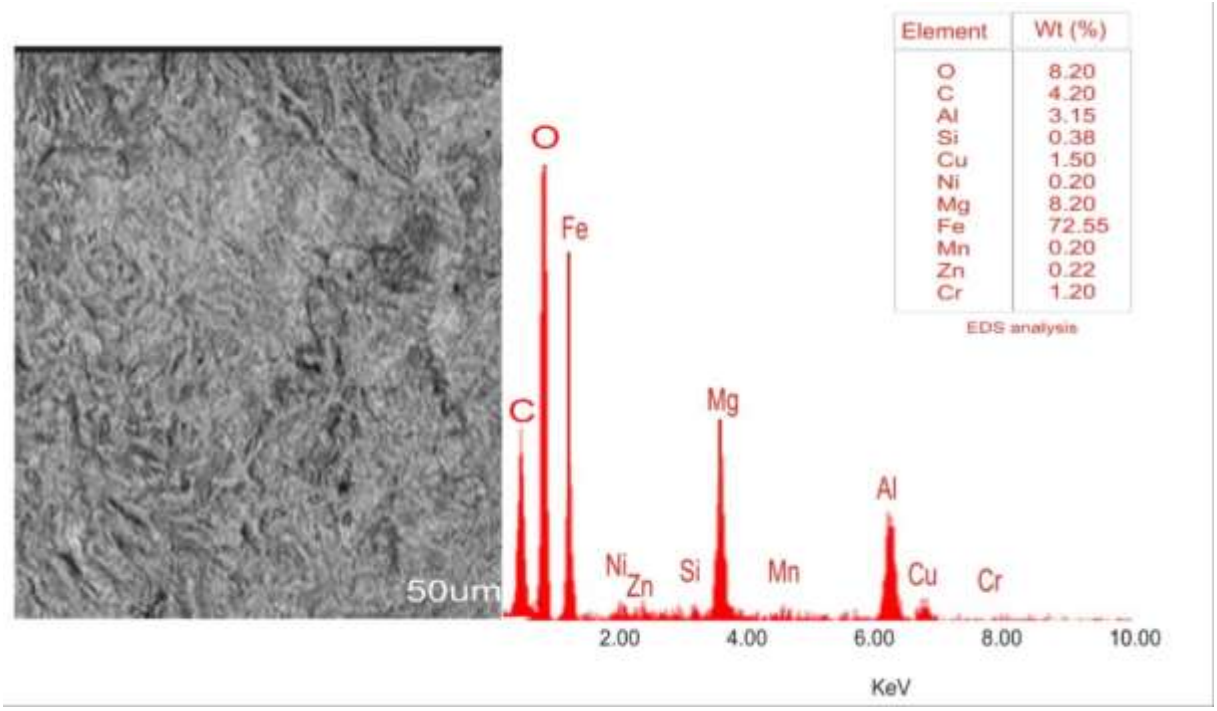

Figure 17: *SEM and EDX data of mild steel immersed in 2.5M HCl without inhibitor.*

In contrast, the steel surface immersed in 2.5 M HCl containing 200 ppm okra leaf extract (Figures 18–19) is markedly improved, appearing comparatively smooth with significantly fewer pits, suggesting effective corrosion suppression. The corresponding EDX spectrum (Figure 19) shows iron as the predominant element, along with additional peaks corresponding to nitrogen (N) and phosphorus (P), which are absent in the uninhibited sample. These heteroatoms are attributed to polyphenols, tannins, organic acids, and nitrogen-containing constituents of the extract, as confirmed by FTIR and GC–MS analyses. Similar observations of heteroatom-mediated adsorption have been reported in studies using plant extracts as corrosion inhibitors. The presence of N and P on the steel surface provides direct evidence of inhibitor adsorption and potential coordination with surface iron atoms, forming a protective organic film.

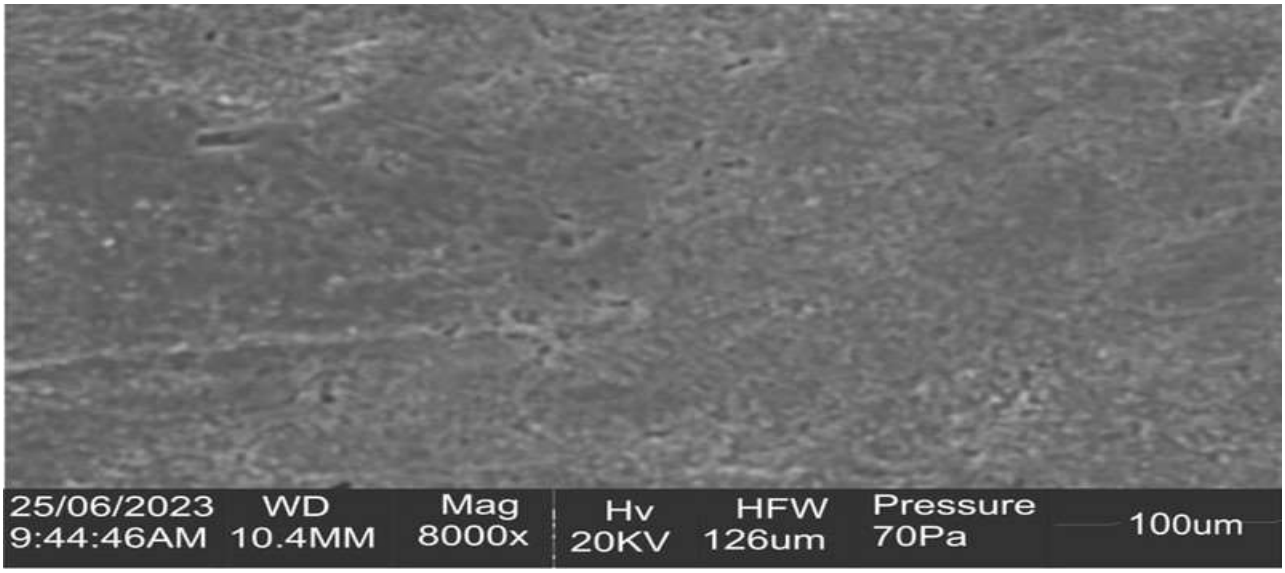

Figure 18: *100µm SEM Micrograph of mild steel dip in 2.5 M HCL medium with inhibitor concentration of 200 ppm.*

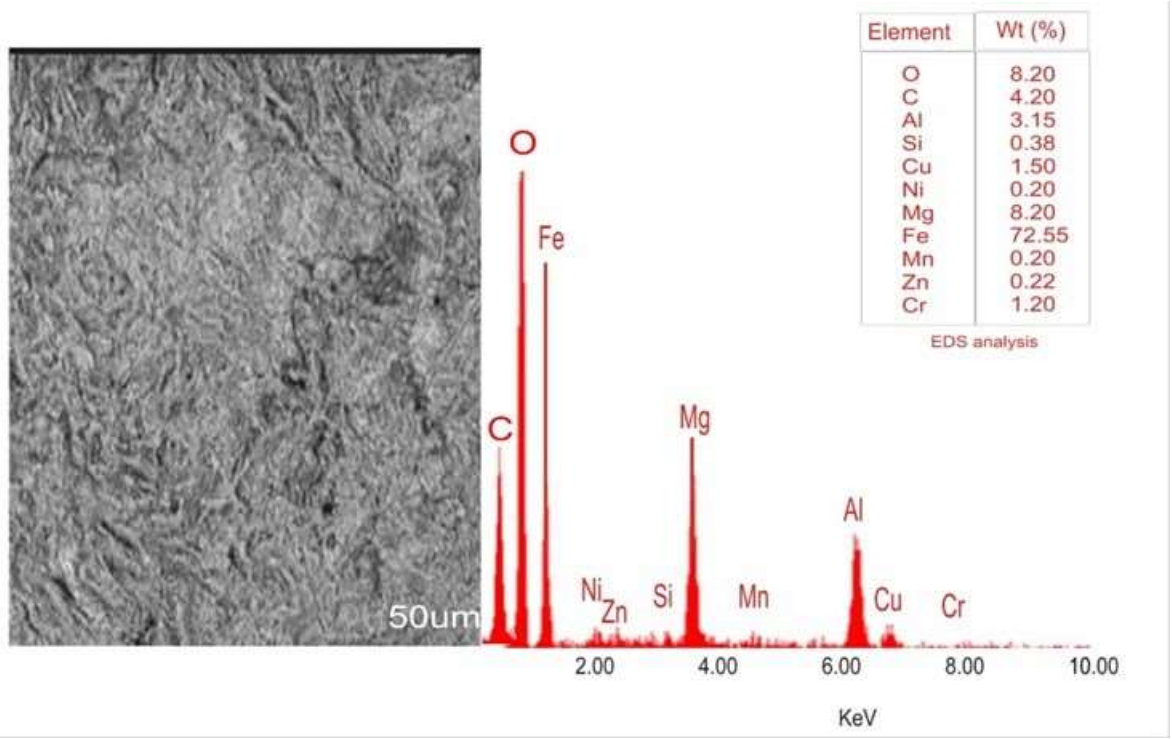

Figure 19: *SEM and EDX data of mild steel immersed in 2.5M HCL with inhibitor concentration of 200ppm*

The intensity of oxygen in the inhibited spectrum is substantially reduced relative to the uninhibited case, indicating that the adsorbed organic layer effectively limits oxygen and chloride access to the metal surface and restricts oxide formation. The remaining oxygen signal is likely due to functional groups within the inhibitor molecules themselves, which serve as adsorption centres anchoring the organic film to the steel surface. This observation supports the notion that corrosion inhibition in this system is dominated by organic film formation rather than oxide-based passivation, a mechanism commonly described for phytochemical corrosion inhibitors [2,14].

The effectiveness of the inhibitor film at 200 ppm corresponds well with potentiodynamic polarization results, which demonstrate reduced corrosion current densities and mixed-type inhibition behaviour. The adherence of the adsorption behaviour to the Langmuir model and moderate activation energy values further suggests a predominantly physical adsorption mechanism, with possible contributions from weak chemisorption. Such behaviour is consistent with previous reports on okra mucilage extracts and other plant extracts under acidic conditions, which also exhibit reduced inhibition efficiency at elevated temperatures due to partial desorption of inhibitor molecules

Overall, the SEM–EDX results (Figures 15–19) provide compelling microstructural and compositional evidence that *A. esculentus* leaf extract forms a stable, adherent protective film on mild steel in acidic environments. This organic layer effectively suppresses both anodic iron dissolution and cathodic hydrogen evolution by reducing the availability of active surface sites, confirming the potential of okra leaf extract as an environmentally benign and efficient corrosion inhibitor for mild steel in hydrochloric acid solutions.

4. CONCLUSION

The study confirmed, through FTIR and GC–MS analyses, the presence of functional groups in *Okro* (Abelmoschus esculentus) leaf extract responsible for corrosion inhibition of mild steel in acidic medium. The inhibitor exhibited significant adsorption capability on the metal surface, forming a stable, protective film that effectively reduced corrosion attack.

The inhibition efficiency decreased with increasing temperature, particularly beyond 60 °C, indicating that the adsorption process was temperature-dependent. Conversely, higher inhibitor concentrations enhanced corrosion resistance, demonstrating a concentration-dependent protective effect. The experimentally observed corrosion rate values were in good agreement with those predicted by the kinetic model.

Thermodynamic evaluations revealed that the activation energy (Ea) and enthalpy of activation (ΔH) were higher for inhibited systems than for the uninhibited ones, implying a reduced corrosion rate due to the formation of an energy barrier by the inhibitor film. The positive ΔH confirmed an endothermic adsorption process, while the negative Gibbs free energy values

(ΔG°ads) indicated spontaneous adsorption of inhibitor molecules onto the steel surface. The lower entropy of activation (ΔS) with increasing acid concentration suggested a more ordered state of the activated complex. Surface analysis using SEM–EDX further validated these findings, revealing the presence of a dense, fibrous protective layer on the steel surface in the presence of 200 ppm *Okro* leaf extract. The adsorption data best fitted the Langmuir isotherm model, indicating monolayer adsorption on a homogeneous surface.

Overall, the *Okro* leaf extract demonstrated excellent corrosion inhibition performance for mild steel in acidic environments, signifying its potential as an effective, eco-friendly green inhibitor for industrial acid-cleaning and pickling applications.

Author Contributions: Conceptualization, A. O. O., J. J. G., T. A. O. and Z. F. A.; methodology, J. J. G., and T.A.O.; validation, J. J. G., Z. F. A., T. A. O., and A. O. O.; formal analysis, J. J. G., T.A.O., and Z. F. A.; investigation, J. J. G., and T.A.O.; data curation, J. J. G., and T.A.O.; writing— J. J. G and T. A. O.; original draft preparation, J. J. G., and T.A.O.; writing—review and editing, T.A.O., J. J. G., and Z. F. A.; supervision, A. O. O.; project administration, Z. F. A.

All authors have read and agreed to the published version of the manuscript.

Funding: *This research did not receive any specific grant from funding agencies in the public, commercial, or not-for-profit sectors*.

Data Availability Statement: The data presented in this study are available on request from the corresponding author. The data are not publicly available due to privacy.

Conflicts of Interest: The authors declare no conflict of interest.

Nomenclature

Symbol	Description	Unit
A	Surface area	cm^2
B_a	Anodic Tafel slope for the half-reaction	$V\ dec^{-1}$
B_c	Cathodic Tafel slope for the half-reaction	$V\ dec^{-1}$
C	Inhibitor concentration	$mol\ L^{-1}$
CR_{blank}	Corrosion rate in the blank solution (without inhibitor)	mpy
CR_{inh}	Corrosion rate in the inhibited solution	mpy
ΔE	Change in potential	V
E	Potential	V
E_a	Activation energy	$J\ mol^{-1}$
E_{corr}	Corrosion potential	V
h	Planck's constant	6.626×10^{-34} J s
I_{anodic}	Anodic current	A
$I_{cathodic}$	Cathodic current	A
I_{corr}	Corrosion current	A
i_{corr}	Corrosion current density in the presence of inhibitor	$A\ cm^{-2}$
I'_{corr}	Corrosion current density in uninhibited solution	$A\ cm^{-2}$
i_{corr}	Corrosion current density	$A\ cm^{-2}$
K_{ads}	Adsorption equilibrium constant	$L\ mol^{-1}$
K_F	Freundlich constant	—
K_T	Equilibrium binding constant	$L\ mol^{-1}$
N	Avogadro's number	$6.022 \times 10^{23}\ mol^{-1}$
n	Adsorption intensity	—
q_m	Monolayer adsorption capacity	$mg\ g^{-1}$
R	Universal gas constant	$8.314\ J\ mol^{-1}\ K^{-1}$
R_p	Polarization resistance	$\Omega\ cm^2$
t	Immersion time	h
T	Absolute temperature	K
W	Weight loss	mg
ΔG_a	Change in Gibbs free energy of activation	$J\ mol^{-1}$
ΔG_{ads}	Gibbs free energy of adsorption	$J\ mol^{-1}$
ΔH	Enthalpy	$J\ mol^{-1}$
ΔH_a	Enthalpy of activation	$J\ mol^{-1}$
ΔH_{ads}	Enthalpy of adsorption	$J\ mol^{-1}$
ΔS	Entropy	$J\ mol^{-1}\ K^{-1}$
ΔS_{ads}	Entropy of adsorption	$J\ mol^{-1}\ K^{-1}$
θ	Surface coverage	—

REFERENCES

[1] Z. Ren, K. Chen, D. Yang, Z. Wang, and W. Qin, 'Predicting the External Corrosion Rate of Buried Pipelines Using a Novel Soft Modeling Technique', Appl. Sci., vol. 14, no. 12, p. 5120, Jun. 2024, doi: 10.3390/app14125120.

[2] A. Elwerfalli, S. Alsadaie, and I. M. Mujtaba, 'Estimation of Shutdown Schedule to Remove Fouling Layers of Heat Exchangers Using Risk-Based Inspection (RBI)', Processes, vol. 9, no. 12, p. 2177, Dec. 2021, doi: 10.3390/pr9122177.

[3] F. Zucchi and I. H. Omar, 'Plant extracts as corrosion inhibitors of mild steel in HCl solutions', Surf. Technol., vol. 24, no. 4, pp. 391–399, 1985.

[4] M. M. Attia, 'RISK BASED INSPECTION (RBI) ASSESSMENT AT ABOVEGROUND STORAGE TANKS (ASTS)'.

[5] P. R. Roberge, Handbook of Corrosion Engineering, Third Edition, 3rd edition. New York, N.Y: McGraw-Hill Education, 2019.

[6] A. Babaeian, A. Eslami, F. Ashrafizadeh, M. A. Golozar, M. Samadzadeh, and F. Abbasian, 'Risk-based inspection (RBI) of a gas pressure reduction station', J. Loss Prev. Process Ind., vol. 84, p. 105100, Sep. 2023, doi: 10.1016/j.jlp.2023.105100.

[7] J. R. Scully, 'Polarization Resistance Method for Determination of Instantaneous Corrosion Rates', Corrosion, vol. 56, no. 2, pp. 199–218, Feb. 2000, doi: 10.5006/1.3280536.

[8] J. C. Reeve and G. Bech-Nielsen, 'The Stern-Geary method. Basic difficulties and limitations and a simple extension providing improved reliability', Corros. Sci., vol. 13, no. 5, pp. 351–359, Jan. 1973, doi: 10.1016/0010-938X(73)90038-3.

[9] F. Ropital, '15 - Environmental degradation in hydrocarbon fuel processing plant: issues and mitigation', in Advances in Clean Hydrocarbon Fuel Processing, M. R. Khan, Ed., Woodhead Publishing, 2011, pp. 437–462. doi: 10.1533/9780857093783.5.437.

[10] M. Stern, 'A Method For Determining Corrosion Rates From Linear Polarization Data', Corrosion, vol. 14, no. 9, pp. 60–64, Sep. 1958, doi: 10.5006/0010-9312-14.9.60.

[11] L. Afia et al., 'Steel Corrosion Inhibition by Acid Garlic Essential Oil as a Green Corrosion Inhibitor and Sorption Behavior', Int. J. Electrochem. Sci., vol. 9, no. 12, pp. 8392–8406, Dec. 2014, doi: 10.1016/S1452-3981(23)11055-8.

[12] 'Inhibition of corrosion of mild steel pipeline carrying simulated oil well water by Allium sativum (garlic) extract', Int. J. Corros. Scale Inhib., vol. 10, no. 3, Sep. 2021, doi: 10.17675/2305-6894-2021-10-3-8.

[13] 'Okewale et al Investigation of the use of ethyl esters of castor'.

[14] A. D. M. Santos, T. F. D. Almeida, F. Cotting, I. V. Aoki, H. G. D. Melo, and V. R. Capelossi, 'Evaluation of Castor Bark Powder as a Corrosion Inhibitor for Carbon Steel in Acidic Media', Mater. Res., vol. 20, no. suppl 2, pp. 492–505, Oct. 2017, doi: 10.1590/1980-5373-mr-2016-0963.

[15] A. O. Alao, A. P. Popoola, M. O. Dada, and O. Sanni, 'Utilization of green inhibitors as a sustainable corrosion control method for steel in petrochemical industries: A review', Front. Energy Res., vol. 10, p. 1063315, Jan. 2023, doi: 10.3389/fenrg.2022.1063315.

[16] S. A. Hussein and A. A. Khadom, 'Okra leaves extract as green corrosion inhibitor for steel in sulfuric acid: Gravimetric, electrochemical, and surface morphological investigations', Results Chem., vol. 8, p. 101566, Jun. 2024, doi: 10.1016/j.rechem.2024.101566.

[17] K. F. Khaled, 'New Synthesized Guanidine Derivative as a Green Corrosion Inhibitor for Mild Steel in Acidic Solutions', Int. J. Electrochem. Sci., vol. 3, no. 4, pp. 462–475, Apr. 2008, doi: 10.1016/S1452-3981(23)15466-6.

[18] S. A. Umoren, O. Ogbobe, I. O. Igwe, and E. E. Ebenso, 'Inhibition of mild steel corrosion in acidic medium using synthetic and naturally occurring polymers and synergistic halide additives', Corros. Sci., vol. 50, no. 7, pp. 1998–2006, Jul. 2008, doi: 10.1016/j.corsci.2008.04.015.

[19] N. I. Kairi and J. Kassim, 'The Effect of Temperature on the Corrosion Inhibition of Mild Steel in 1 M HCl Solution by Curcuma Longa Extract', Int. J. Electrochem. Sci., vol. 8, no. 5, pp. 7138–7155, May 2013, doi: 10.1016/S1452-3981(23)14836-X.

[20] Z. Yi, J. Yao, M. Zhu, H. Chen, F. Wang, and X. Liu, 'Kinetics, equilibrium, and thermodynamics investigation on the adsorption of lead(II) by coal-based activated carbon', SpringerPlus, vol. 5, no. 1, p. 1160, Jul.

2016, doi: 10.1186/s40064-016-2839-4.

[21] M. Oki, C. Ebitei, C. Alaka, and T. K. Oki, ‘Corrosion inhibition of mild steel in hydrochloric acid by tannins from Rhizophora racemosa’, Mater. Sci. Appl., vol. 2, pp. 592–595, 2011.

[22] K. Rajam, S. Rajendran, and R. Saranya, ‘Allium Sativum (Garlic) Extract as Nontoxic Corrosion Inhibitor’, J. Chem., vol. 2013, no. 1, p. 743807, Jan. 2013, doi: 10.1155/2013/743807.

[23] D. Yawas, ‘Suitability assessment of some plant extracts and fatty acid vegetable oil as corrosive inhibitors’, 2005.

[24] R. Saratha, S. Priya, and P. Thilagavathy, ‘Investigation of Citrus aurantiifolia leaves extract as corrosion inhibitor for mild steel in 1 M HCl’, J. Chem., vol. 6, no. 3, pp. 785–795, 2009.

[25] A. Toghan, H. S. Gadow, A. Fawzy, H. Alhussain, and H. Salah, ‘Adsorption Mechanism, Kinetics, Thermodynamics, and Anticorrosion Performance of a New Thiophene Derivative for C-Steel in a 1.0 M HCl: Experimental and Computational Approaches’, Metals, vol. 13, no. 9, 2023, doi: 10.3390/met13091565.

[26] J. Nwabanne and V. Okafor, ‘Inhibition of the corrosion of mild steel in acidic medium by Vernonia amygdalina: adsorption and thermodynamics study’, J. Emerg. Trends Eng. Appl. Sci., vol. 2, no. 4, pp. 619–625, 2011.

[27] A. Miralrio and A. Espinoza Vázquez, ‘Plant extracts as green corrosion inhibitors for different metal surfaces and corrosive media: a review’, Processes, vol. 8, no. 8, p. 942, 2020.

[28] M. Mohamed-Said, B. Vuillemin, R. Oltra, A. Marion, L. Trenty, and D. Crusset, ‘Predictive modelling of the corrosion rate of carbon steel focusing on the effect of the precipitation of corrosion products’, Corros. Eng. Sci. Technol., vol. 52, no. 1_suppl, pp. 178–185, 2017.

[29] R. Abd El-Hameed, ‘Aminolysis of polyethylene terephthalate waste as corrosion inhibitor for carbon steel in HCl corrosive medium’, Adv. Appl. Sci. Res., vol. 2, no. 3, pp. 483–499, 2011.

[30] N. Eddy, S. Odoemelam, and A. Odiongenyi, ‘Ethanol extract of Musa species peels as a green corrosion inhibitor for mild steel: kinetics, adsorption and thermodynamic considerations.’, 2009.

[31] Y. Qiang, L. Guo, H. Li, and X. Lan, ‘Fabrication of environmentally friendly Losartan potassium film for corrosion inhibition of mild steel in HCl medium’, Chem. Eng. J., vol. 406, p. 126863, 2021.

[32] A. Zarrouk, B. Hammouti, H. Zarrok, S. Al-Deyab, and M. Messali, ‘Temperature effect, activation energies and thermodynamic adsorption studies of L-cysteine methyl ester hydrochloride as copper corrosion inhibitor in nitric acid 2M’, Int. J. Electrochem. Sci., vol. 6, no. 12, pp. 6261–6274, 2011.

[33] N. Ayawei, A. N. Ebelegi, and D. Wankasi, ‘Modelling and interpretation of adsorption isotherms’, J. Chem., vol. 2017, no. 1, p. 3039817, 2017.

[34] A. Kokalj, ‘On the use of the Langmuir and other adsorption isotherms in corrosion inhibition’, Corros. Sci., vol. 217, p. 111112, 2023.

[35] M. Vuković, B. Pesic, N. Štrbac, I. Mihajlović, and M. Sokić, ‘Linear polarization study of the corrosion of iron in the presence of Thiobacillus ferrooxidans bacteria’, Int. J. Electrochem. Sci., vol. 7, no. 3, pp. 2487–2503, 2012.

[36] M. Abdallah, M. Salem, B. Jahdaly, M. Awad, E. Helal, and A. Fouda, ‘Corrosion inhibition of stainless steel type 316 L in 1.0 M HCl solution using 1, 3-thiazolidin-5-one derivatives’, Int. J. Electrochem. Sci., vol. 12, no. 5, pp. 4543–4562, 2017.

[37] S. N. N. M. Makhtar et al., ‘Preparation, characterization and performance evaluation of supported zeolite on porous glass hollow fiber for desalination application’, Arab. J. Chem., vol. 13, no. 1, pp. 3429–3439, 2020.